AFRL-RX-WP-JA-2016-0344

AMORPHOUS BORON NITRIDE: A UNIVERSAL, ULTRATHIN DIELECTRIC FOR 2D NANOELECTRONICS (POSTPRINT)

N.R. Glavin, M.L. Jespersen, J. Hu, P.T. Hagerty, Al M. Hilton, A.T. Blake, C.A. Grabowski, and Dr. M.F. Durstock,
AFRL/RX

T.S. Fisher
Purdue University

C. Muratore
University of Dayton

DM.L. Jespersen, J. Hu, and P. T. Hagerty
University of Dayton Research Laboratory

A.M. Hilton
Wyle

C.A. Grabowski   A.A. Voevodin
UES   University of North Texas

17 November 2015
Interim Report

(STINFO COPY)
AIR FORCE RESEARCH LABORATORY
MATERIALS AND MANUFACTURING DIRECTORATE
WRIGHT-PATTERSON AIR FORCE BASE, OH 45433-7750
AIR FORCE MATERIEL COMMAND
UNITED STATES AIR FORCE

REPORT DOCUMENTATION PAGE

Form Approved
OMB No. 0704-0188

1. REPORT DATE *(DD-MM-YY)*	2. REPORT TYPE	3. DATES COVERED *(From - To)*
17 November 2015	Interim	29 January 2013 – 17 October 2015

4. TITLE AND SUBTITLE
AMORPHOUS BORON NITRIDE: A UNIVERSAL, ULTRATHIN DIELECTRIC FOR 2D NANOELECTRONICS (POSTPRINT)

5a. CONTRACT NUMBER
FA8650-11-D-5401-0011

5b. GRANT NUMBER

5c. PROGRAM ELEMENT NUMBER
62102F

6. AUTHOR(S)
1) N.R. Glavin, M.L. Jespersen, J. Hu, P.T. Hagerty, Al M. Hilton, A.T. Blake, C.A. Grabowski, and Dr. M.F. Durstock, AFRL/RX

2) T.S. Fisher – Purdue University

(continued on page 2)

5d. PROJECT NUMBER
4347

5e. TASK NUMBER 0011

5f. WORK UNIT NUMBER
X0K9

7. PERFORMING ORGANIZATION NAME(S) AND ADDRESS(ES)
1) AFRL/RX
Wright-Patterson AFB, OH 45433

2) Purdue University
Hovde HaWest Lafayette, IN 47907

(continued on page 2)

8. PERFORMING ORGANIZATION REPORT NUMBER

9. SPONSORING/MONITORING AGENCY NAME(S) AND ADDRESS(ES)
Air Force Research Laboratory
Materials and Manufacturing Directorate
Wright-Patterson Air Force Base, OH 45433-7750
Air Force Materiel Command
United States Air Force

10. SPONSORING/MONITORING AGENCY ACRONYM(S)
AFRL/RXAS

11. SPONSORING/MONITORING AGENCY REPORT NUMBER(S)
AFRL-RX-WP-JA-2016-0344

12. DISTRIBUTION/AVAILABILITY STATEMENT
Distribution Statement A. Approved for public release: distribution unlimited.

13. SUPPLEMENTARY NOTES
PA Case Number: 88ABW-2015-5638; Clearance Date: 17 Nov 2015. This document contains color. Journal article published in Advanced Functional Material, Vol. 26, No. 16, 25 Apr 2016. © 2016 Wiley-VCH. The U.S. Government is joint author of the work and has the right to use, modify, reproduce, release, perform, display, or disclose the work. The final publication is available at www.afm-journal.de DOI: 10.1002/adfm.201505455

14. ABSTRACT *(Maximum 200 words)*
Next-generation nanoelectronics based on 2D materials ideally will require reliable, flexible, transparent, and versatile dielectrics for transistor gate barriers, environmental passivation layers, capacitor spacers, and other device elements. Ultrathin amorphous boron nitride of thicknesses from 2 to 17 nm, described in this work, may offer these attributes, as the material is demonstrated to be universal in structure and stoichiometric chemistry on numerous substrates including flexible polydimethylsiloxane, amorphous silicon dioxide, crystalline Al_2O_3, other 2D materials including graphene, 2D MoS_2, and conducting metals and metal foils. The versatile, large area pulsed laser deposition growth technique is performed at temperatures less than 200 °C and without modifying processing conditions, allowing for seamless integration into 2D device architectures. A device-scale dielectric constant of 5.9 ± 0.65 at 1 kHz, breakdown voltage of 9.8 ± 1.0 MV cm^{-1}, and bandgap of 4.5 eV were measured for various thicknesses of the ultrathin a-BN material, representing values higher than previously reported chemical vapor deposited h-BN and nearing single crystal h-BN.

15. SUBJECT TERMS
Nanoelectronics; 2D materials; dielectrics; transistor gate barriers; environmental passivation layers; boron nitride; h-BN

16. SECURITY CLASSIFICATION OF:

a. REPORT	b. ABSTRACT	c. THIS PAGE	17. LIMITATION OF ABSTRACT:	18. NUMBER OF PAGES	19a. NAME OF RESPONSIBLE PERSON (Monitor)
Unclassified	Unclassified	Unclassified	SAR	11	Nicholas Glavin
					19b. TELEPHONE NUMBER *(Include Area Code)* (937) 255-6977

Standard Form 298 (Rev. 8-98)
Prescribed by ANSI Std. Z39-18

REPORT DOCUMENTATION PAGE Cont'd

6. AUTHOR(S)

   3) C. Muratore - UD

   4) DM.L. Jespersen, J. Hu, and P. T. Hagerty - UDRL

   5) A.M. Hilton – Wyle

   6) C.A. Grabowski - UES

   7) A.A. Voevodin - University of North Texas

7. PERFORMING ORGANIZATION NAME(S) AND ADDRESS(ES)

   3) University of Dayton, 300 College Park, Dayton,
      OH 45409

   4) University of Dayton Research Laboratory
      1801 S Edwin C Moses Blvd Dayton, OH 45417

   5) Wyle Laboratories, 4200 Colonel Glenn Hwy,
      Beavercreek Township, OH 45431

   6) UES Inc., 4401 Dayton Xenia Rd, Beavercreek, OH
      45432

   7) University of North Texas, 1155 Union Circle,
      #311277, Denton, TX 76203

FULL PAPER

Amorphous Boron Nitride: A Universal, Ultrathin Dielectric For 2D Nanoelectronics

Nicholas R. Glavin,* Christopher Muratore, Michael L. Jespersen, Jianjun Hu, Phillip T. Hagerty, Al M. Hilton, Austin T. Blake, Christopher A. Grabowski, Michael F. Durstock, Michael E. McConney, Drew M. Hilgefort, Timothy S. Fisher, and Andrey A. Voevodin

Next-generation nanoelectronics based on 2D materials ideally will require reliable, flexible, transparent, and versatile dielectrics for transistor gate barriers, environmental passivation layers, capacitor spacers, and other device elements. Ultrathin amorphous boron nitride of thicknesses from 2 to 17 nm, described in this work, may offer these attributes, as the material is demonstrated to be universal in structure and stoichiometric chemistry on numerous substrates including flexible polydimethylsiloxane, amorphous silicon dioxide, crystalline Al_2O_3, other 2D materials including graphene, 2D MoS_2, and conducting metals and metal foils. The versatile, large area pulsed laser deposition growth technique is performed at temperatures less than 200 °C and without modifying processing conditions, allowing for seamless integration into 2D device architectures. A device-scale dielectric constant of 5.9 ± 0.65 at 1 kHz, breakdown voltage of 9.8 ± 1.0 MV cm^{-1}, and bandgap of 4.5 eV were measured for various thicknesses of the ultrathin a-BN material, representing values higher than previously reported chemical vapor deposited h-BN and nearing single crystal h-BN.

1. Introduction

Applications for 2D materials and their heterostructures in fields such as communications, high speed computing, sensing, and energy harvesting are currently limited by the absence of direct and repeatable synthesis methods for cost effective device fabrication. While conducting (e.g., graphene,

TaS_2), and semiconducting (e.g., MoS_2, WS_2) 2D materials are being rapidly advanced for next-generation 2D devices,[1–6] ultrathin and high strength dielectric materials for transistor gates, capacitors, memory devices, and barrier layers for electrical and ambient environment isolation are far less developed. This circumstance is primarily a result of the fundamental challenge in synthesis of ultrathin insulating materials at moderate temperatures (<900 °C) needed for direct growth over large lateral dimensions.[7] In silicon-based electronics, silicon dioxide (SiO_2) has proven to be an ideal dielectric material due to the large band gap (9 eV), well-matched interfacial properties with silicon, and simple, repeatable processing. Synthesis routes including thermal decomposition of Si[8] and plasma enhanced chemical vapor deposition (PECVD) have been extensively studied and are now routine industrial operations. While integration of SiO_2 on silicon-based devices is commonplace, synthesis of ultrathin dielectrics with interfacial characteristics suitable for use with diverse (i.e., electrically insulating and conducting) 2D materials, without compromising unique 2D benefits such as optical transparency and mechanical flexibility, is critical for realization of flexible electronic devices and other premium

N. R. Glavin, Dr. M. L. Jespersen, Dr. J. Hu, P. T. Hagerty,
Dr. A. M. Hilton, A. T. Blake, Dr. C. A. Grabowski, Dr. M. F. Durstock,
Dr. M. E. McConney, D. M. Hilgefort
Materials and Manufacturing Directorate
Air Force Research Laboratory
Wright-Patterson AFB
OH 45433, USA
E-mail: Nicholas.Glavin.1@us.af.mil
N. R. Glavin, Prof. T. S. Fisher
School of Mechanical Engineering and Birck Nanotechnology Center
Purdue University
West Lafayette, IN 47907, USA
Prof. C. Muratore
University of Dayton
Dayton, OH 45409, USA

Dr. M. L. Jespersen, Dr. J. Hu, P. T. Hagerty,
D. M. Hilgefort
University of Dayton Research Laboratory
Dayton, OH 45409, USA
Dr. A. M. Hilton
Wyle Laboratories
Dayton, OH 43433, USA
Dr. C. A. Grabowski
UES Inc.
Dayton, OH 45432, USA
Prof. A. A. Voevodin
Materials Science and Engineering
University of North Texas
Denton, TX 76203, USA

1

Makrials
Views
www.MaterialsViews.com

**ADVANCED
FUNCTIONAL
MATERIALS**
www.afm-journal.de

FULL PAPER

areas of nanotechnological innovation. Atomic layer deposition of HfO_2[9,10] and Al_2O_3,[11] thermal activated growth of h-BN by CVD, and other alternatives to SiO_2 are some of the recently reported direct-growth approaches that suffer from significant scaling, process tuning, and pinhole-free uniformity challenges.

Ultrathin boron nitride films are especially attractive as a candidate dielectric material in 2D material systems. In the crystalline hexagonal form (h-BN), the boron nitride sheet is isostructural to that of graphene, differing in lattice spacing by only 1.8%.[12] In contrast to graphene, the mainly ionic nature of the B—N bond results in a wide band gap near 5 eV, which is consistent among the amorphous, hexagonal, and cubic allotropes of BN.[13–16] The chemical and structural stability of BN at high temperatures[17] make synthesis of continuous, high quality crystalline hexagonal or cubic BN phases over appreciable lateral dimensions a challenge. In addition, the recent desire for mono- or few-layer h-BN in high speed electronic devices has proven difficult, as the hexagonal phase is the higher temperature phase of BN.[18]

Chemical vapor deposition (CVD) is the most widely used direct synthesis method, suitable for use over large areas, of ultrathin h-BN,[19] and involves thermal decomposition of boron- and nitrogen-containing precursor gases on a heated substrate. Using this method, monolayer h-BN was first synthesized at high temperatures (typically > 900 °C) in isolated triangular[20,21] or hexagonal[22] domains with characteristic lengths of a few micrometers on transition metal foils including Cu,[22,23] Ni,[24] and later, others.[25–29] Prior studies reveal that the thermally activated CVD processes for high quality, 2D h-BN growth are strongly substrate-dependent, and require substantial tailoring to accommodate the full range of chemical reactivities and surface energies of the substrate material. Recent progress in direct growth methods of h-BN has been reported on insulating Al_2O_3 (0001) and conducting Si (111) using a two-step process of pregrowth annealing at 1000 °C followed by the decomposition of polyborazylene precursor, representing a key advance in few-layer h-BN growth prospects.[30] Ideally, a versatile synthesis route that facilitates nucleation and coalescence of continuous ultrathin BN insulating films on all electronic materials of interest (metal, ceramics, polymers, graphene, and other 2D materials) at temperatures <200 °C, without the requirement of tuning the deposition conditions for every substrate of interest, would facilitate simple integration of ultrathin dielectrics into 2D devices.

2. Results and Discussion

For both conducting and semiconducting 2D materials, well-ordered structure is essential to obtain the desired electronic, optical, and mechanical properties, as these are dictated by the anisotropy of interatomic bonding arrangements and electron density distributions, which are unique for such 2D materials. This structural anisotropy could be much less essential, however, for wide bandgap materials with no electrons in the conduction band, such as BN. Thus, if (a) atomic order is not necessary to obtain the desired dielectric properties for ultrathin insulating materials based on BN, and (b) the film growth can be activated by nonthermal means, then the synthesis temperatures can be reduced to allow for direct, large area growth and thus to enable flexible cost-effective 2D device production. The approach described here utilizes a low temperature (<200 °C) pulsed laser deposition (PLD) of ultrathin BN dielectric films as a universal means of direct growth of pinhole-free, few-nanometer-thick and high dielectric strength films on a number of metal, ceramic, and polymer substrates as well as on the surface of 2D materials including graphene and few-layer MoS_2.

Table 1 compares physical properties of various insulating BN materials (from bulk to ultrathin) to that of thermally grown SiO_2. Bulk amorphous boron nitride is characterized by predominantly sp^2 bonding, is transparent and insulating, and is typically used as an intermediate layer in c-BN synthesis processes in prior works.[13,31] The reported measured electronic properties of these thin film a-BN (films with thickness >600 nm) are nearly identical to thermal activated growth of h-BN by CVD, in terms of measured dielectric strength, dielectric constant, and bandgap energy values (see Table 1). The amorphous material possesses a density similar to the crystalline phases, and retains much of the valued chemical inertness and high thermal stability characteristics of its hexagonal counterpart. The electronic properties of a-BN where the device measurements were made (6 and 17 nm) described throughout this work are reported in the final column of Table 1 and will be discussed later.

Amorphous boron nitride with a controllable thickness of 2–17 nm was synthesized using a pulsed laser deposition method optimized for ultrathin growth. A comprehensive description of the process development can be found in prior work.[38,39] Briefly, a 248 nm KrF pulsed UV laser enters a nitrogen filled vacuum chamber through a focusing lens and strikes a rotating boron nitride target, as seen in a schematic

Table 1. Comparison of electronic properties of thin film a-BN, CVD deposited h-BN, single crystal h-BN, and thermally grown SiO_2.

Property	Thin film (>600 nm) a-BN	CVD h-BN[a]	Single crystal h-BN	Thermal SiO_2	Ultrathin a-BN (this work)
Density	2.28	–	2.0–2.28[32]	2.27[8]	–
Dielectric constant	≈3.5[14]	3 ± 1.0[33]	6.85[32]	3.9[8]	5.9 ± 0.7
Dielectric strength (MV cm^{-1})	2.2–5.0[13,14]	2–3.8[33,34]	7.9–12 (exfoliated)[35,36]	9 ± 1.0[37]	9.8 ± 1.0
Bandgap (eV)	3.8–5.05[13,14]	5.92[19]	5.2–5.9[15]	≈9[8]	4.5
Direct growth synthesis temperature and compatibility	Typically 200–600 °C, By-product of desired c-BN synthesis	CVD at >900 °C, refractory metal foils and some insulators	Exfoliation required to create ultra-thin layers	Thermal decomposition of silicon at >700 °C	<200 °C, wide range of substrates

[a]Measured dielectric constant and strength of CVD h-BN of thickness ≈15–19 nm.
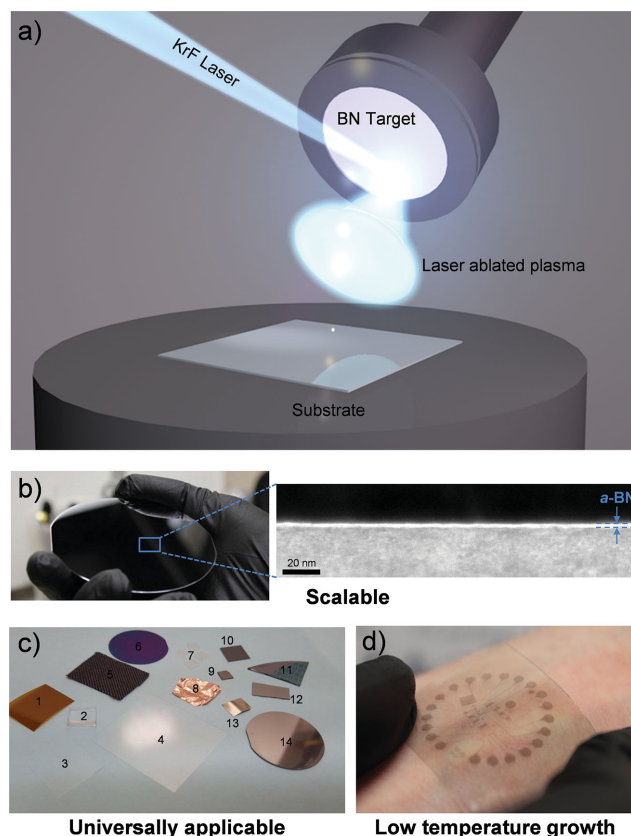
Figure 1. a) Schematic representation of the pulsed laser deposition setup, b) *a*-BN grown on a 3 in. SiO$_2$/Si wafer and cross-sectional TEM of *a*-BN on Al$_2$O$_3$ showing large area uniformity, c) ultrathin a-BN applied to diverse substrates, including (1. Kapton, 2. PDMS, 3. Willow glass, 4. PET, 5. Carbon cloth, 6. SiO$_2$/Si, 7. Al$_2$O$_3$, 8. Copper foil, 9. HOPG, 10. SiC, 11. Patterned SiO$_2$, 12. E-beam evaporated chromium, 13. Nickel foil, 14. Magnetron sputtered tungsten), and d) device construct with directly grown *a*-BN and PVD MoS$_2$ on flexible PET substrate with magnetron sputtered tungsten contacts.

in **Figure 1**a. The nonequilibrium, localized heating of the target surface with the laser beam rapidly vaporizes boron and nitrogen species and in so doing, a high energy plasma is formed. Previously performed spectroscopic studies[39] indicate that the plasma flux extending from the target is composed of ionized boron (B$^+$), ionized nitrogen (N$^+$), neutral excited nitrogen (N*), and a relatively smaller presence of molecular species including N$_2$, N$_2^+$, and BN. The concentrations and time dependent peak occurrences are controlled by laser power density, background gas pressure and the separation, or "working", distance from target to substrate. A combination of the latter two parameters defines the collisional deceleration of the plasma species ablated from the BN target, altering the species' energies and timescales of interactions within the plasma before their arrival to the condensation surface. Element specific plasma composition mapping as a function of both distance from the target and time after the laser pulse was used to identify that the predominant mechanism for formation of stoichiometric BN is the surface recombination of ionized B$^+$ and excited N* species generated at the laser ablated target surface. These particular species reach the substrate location

before other species at 1–2 µs after the laser pulse, and their concentration was maximized for the background gas pressure of 50 mTorr and a working distance of 3 cm used in the current study. Subsequently arriving species, such as molecular N$_2^+$ and atomic N$^+$ ions that are formed due to the background gas decomposition and ionization do not play a significant role in the formation of BN films. The arrival times, concentrations, plasma reactions, and surface growth uniformity are further tuned by optimization of laser power density and other processing parameters, including substrate rotation and beam scanning to facilitate a large area growth.[38,39] Benefits of this optimized PLD approach include the inherent ability to commercialize PLD processes to large areas,[40,41] (Figure 1b shows *a*-BN grown on a Si/SiO$_2$ wafer with a cross-section from a similar wafer), stoichiometric *a*-BN growth at significantly reduced temperatures from room temperature to 200 °C on a diverse range of substrates (Figure 1c), and all without modifying the required deposition conditions.

Figure 2 displays eight cross sectional transmission electron microscopy (TEM) images of the ultrathin *a*-BN films grown on metals (W, Cu foil), insulators (SiO$_2$, Al$_2$O$_3$), other 2D materials (MoS$_2$ and graphene), and polymer substrates (polyethylene terephthalate (PET) and polydimethylsiloxane (PDMS)). All films were synthesized at <200 °C without changing any of the *a*-BN deposition parameters (e.g., nitrogen pressure, working distance, laser power, etc. were kept the same), highlighting the versatility and ease of the deposition technique for growth on electrical conductors, insulators, and semiconductors. The presented BN films represented are of thicknesses from 1–5 nm, which is controlled with at least 0.5 nm precision by the number of laser pulses impacting the target material. Under such process control, *a*-BN with uniform thickness over areas as large as 3 in. can be feasibly synthesized (Figure 1c), as PLD has been shown to enable scale-up with processes such as laser beam rastering[40] and other advanced techniques.[41] Additionally, the wafer-scale, direct synthesis approach eliminates limitations associated with alternative transfer processes (via introduction of structural or chemical defects) or high substrate temperature requirements for BN growth in 2D device production. Amorphous BN films were found to be equally uniform and conformal at thicknesses greater than approximately 2 nm on a local scale, and 6 nm on a device-level scale on tested substrates of 1" in diameter, with no evidence of cross thickness defects (e.g., pinholes or domain boundaries), as confirmed by large area atomic force microscopy (AFM) scans, dielectric measurements at multiple sample locations, and random probing with cross-sectional TEM studies. The amorphous nature of the films is confirmed by Raman, X-ray photoelectron spectroscopy (XPS), and TEM studies, as no evidence of any hexagonal or cubic crystallographic signatures are revealed.

The density and composition of ultrathin *a*-BN films are expected to dictate their insulating properties, as there are no domain boundaries or other well-defined structural features (as shown in Figure 1b). The B:N ratio directly influences dielectric behavior, as nitrogen deficiencies promote metallic B—B bonding that can open conductive pathways or mid-gap states in the band structure of the ultrathin films. High-resolution XPS data seen in **Figure 3** (collected ex situ) indicates excellent stoichiometry and homogeneous bonding chemistry within
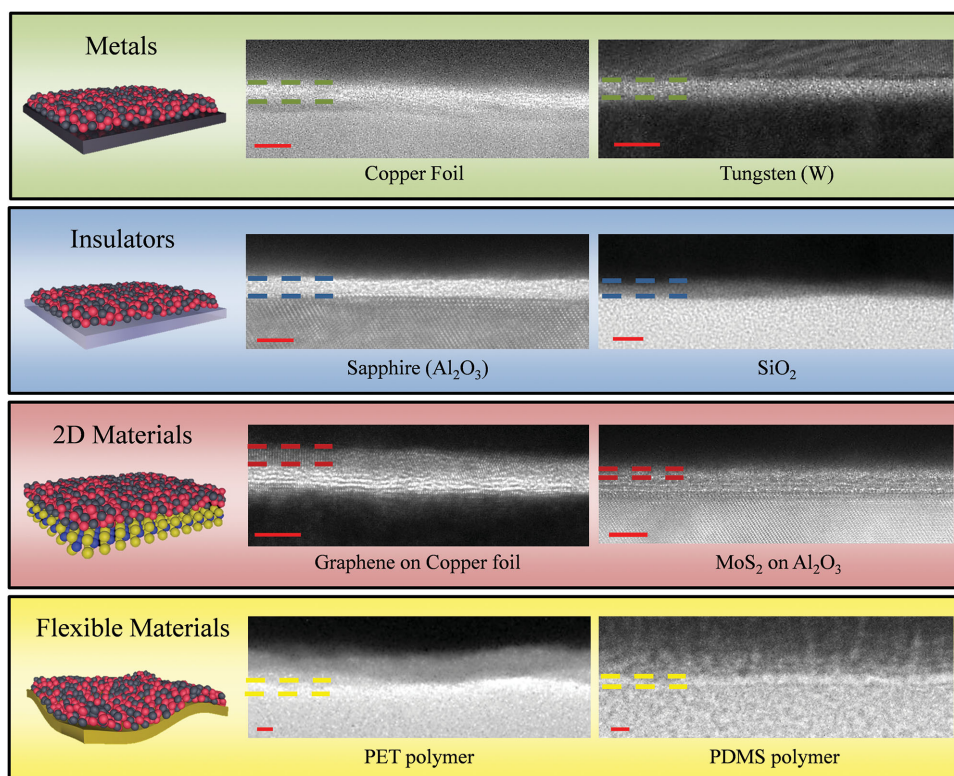
Figure 2. Cross-sectional TEM imaging of amorphous boron nitride growth from room temperature to 200 °C on metal, insulating, 2D material, and flexible substrates (with gold cap layers on top of BN), dotted lines are to aid the reader in identifying *a*-BN material location. Larger area cross-sectional TEMs can be seen in Figure S1 in the Supporting Information.

<5 nm *a*-BN films grown on four substrates having diverse electronic properties and surface energies (from 19.8 mJ m^{-2} for PDMS to >60 mJ m^{-2} for tungsten). Single-component B *1s* (190.6 eV) and N *1s* (398.2 eV) photoelectron peaks indicate B—N bonding, independent of the substrate material. In all cases, the *a*-BN films are nearly stoichiometric with no evidence of metallic B—B bonding (B *1s* ≈ 187 eV[42]) or bonding with the substrate material. We attribute the absence of film-substrate bonds to plasma processing conditions that generate abundant N atoms and ions at the surface and promote nitrogen integration at the film interface.[39]

Homogeneous nucleation and coalescence of ultrathin *a*-BN are driven primarily by the inert nature and resulting low surface energy as compared to the substrate materials, facilitating continuous film formation by the reduction of the condensation surface energy during the film growth. Indicated in Figure 3, the films are stoichiometric on each of the examined substrates as the B:N ratio is near 1:1 and found to be uniform over large areas, confirmed by random sampling of XPS data collection. While uniform growth occurs on all substrates shown in Figure 1c, the initial nucleation stage and deposition rate are, as expected, highly dependent upon the substrate surface energy. Surfaces with a higher surface energy (such as metals) were found to delay the continuous *a*-BN film formation. However after a critical thickness >1–2 nm films on all substrates are continuous and the growth rate is subsequently linear.

The initial growth mechanism proposed for *a*-BN films is two-stage, evidenced by two independent studies employing 2D MoS$_2$ produced by physical vapor deposition[43] and tungsten substrates. PVD-grown MoS$_2$ was covered with *a*-BN films, where film thickness was controlled by varying the number of laser pulses. Ex situ XPS studies reveal significant oxidation of the few-layer MoS$_2$ for *a*-BN overlayers of less than 1 nm thickness
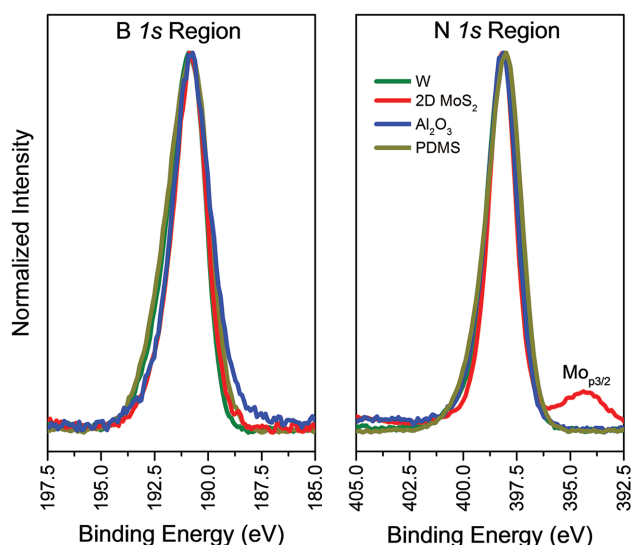

Figure 3. XPS B *1s* and N *1s* regions of <5 nm a-BN films grown at <200 °C on four representative substrates including magnetron sputtered tungsten (W), 2D PVD MoS$_2$, Al$_2$O$_3$, and PDMS.

**ADVANCED
FUNCTIONAL
MATERIALS**

www.afm-journal.de

*Materials
Views*

www.MaterialsViews.com

(achieved with under 20 laser pulses on the BN target). Once the *a*-BN films reached 1 nm or thicker (TEM of *a*-BN on MoS$_2$ from Figure 2 is at 20 pulses), the MoS$_2$ oxidation rate dropped substantially (40% oxidized noncovered versus no apparent oxidation with 1 nm *a*-BN, after 1 week ambient), indicating the minimum number of pulses to reach full coverage of underlying layers is achieved on a large probing area. The proposed initial island nucleation mechanism is also confirmed by localized current–voltage (IV) curves, shown in **Figure 4**a, performed using through-thickness C-AFM of *a*-BN on magnetron sputtered tungsten and a measuring technique similar to Lee et al.[35] The initial growth stage films (produced at <20 pulses) demonstrate small pinholes within the ultrathin layer, evidenced by areas of high conduction seen in Figure 4b. The similarity of the IV curves for the 2–20 pulse growth samples indicate that there is not much change in thickness, as small gaps and pinholes are preferentially filled during the initial growth stage. Once full surface coverage of *a*-BN is achieved (>20 pulses or 1.67 nm), the breakdown potential dramatically increases (Figure 4a), and the film is found to be cohesive, with no evidence of pinholes present on a microscopic area, as indicated in Figure 4c. Beyond this initial nucleation and coalescence stage, the *a*-BN growth enters

uniform growth mode, where subsequent laser pulses result in increased thicknesses and corresponding film breakdown voltages as the deposition rate becomes linearly dependent on the number of laser pulses. Topographical AFM scans of *a*-BN on Al$_2$O$_3$ can be seen in Figure S2, Supporting Information, where the locations of these scans were taken in five locations spaced 5 mm apart on a 30 mm sample surface.

Beginning at the point of coalescence, the measurement of dielectric breakdown strength for films over a range of thicknesses was completed with the C-AFM technique using the linear breakdown method when the current reaches 1 nA.[44] The breakdown is characterized by a sharp increase in current as the electronic behavior enters a regime commonly analyzed using Fowler–Nordheim tunneling theory. The dielectric breakdown strength measured from C-AFM curves at the nearly fully formed samples (<20 pulses) is near 5 MV cm^{-1}, and an increase in the dielectric breakdown to 9.8 ± 1.0 MV cm^{-1} is observed in the fully coalesced 2.2 and 3.1 nm samples (corresponding to 30 and 50 laser pulses, respectively). This value is substantially higher than the breakdown voltage measured in thicker (20 nm) CVD *h*-BN films and approaching the values for that of mechanical exfoliated, single crystal *h*-BN flakes of similar thicknesses.

While C-AFM studies can provide insights into initial growth mechanisms as well as intrinsic material properties, pulsed laser deposited *a*-BN is uniform and cohesive over much larger areas on all tested substrates and amenable to wafer-scale testing. To demonstrate the large area applicability and device production applicability, a simple back-gated device was fabricated using *a*-BN as the active resistor material, a tungsten bottom electrode, and Ti/Au contacts, as shown in the schematic of **Figure 5**a. Fabrication of these devices was conducted in a single chamber and not in a cleanroom facility, highlighting all-PVD direct growth advantage with no transfer/lift off or lithography required to avoid introduction of contamination or other defects. Top contacts of Ti/Au pads were deposited using a TEM mesh, where the contact pads were 40 µm × 40 µm, as shown in Figure 5a. A cross-sectional view of the 6.0 nm thick *a*-BN integrated into the device appears in Figure 5b and a 16.5 nm *a*-BN in Figure S1 in the Supporting Information. The resistivity measurements in devices with thinner *a*-BN samples were insulating, but less so than the reported resistivities for various phases of BN (10^{13}–10^{15} ohm·cm)[45] as pathways through ultrathin insulators at areas of 1600 µm^2 are predominantly caused by extrinsic effects such as dust particles and substrate topography imperfections that induce microscopic leakage pathways. The performance is believed to be amenable to improvement by additional cleaning procedures, as well as processing in a cleanroom facility. Beyond this critical thickness,
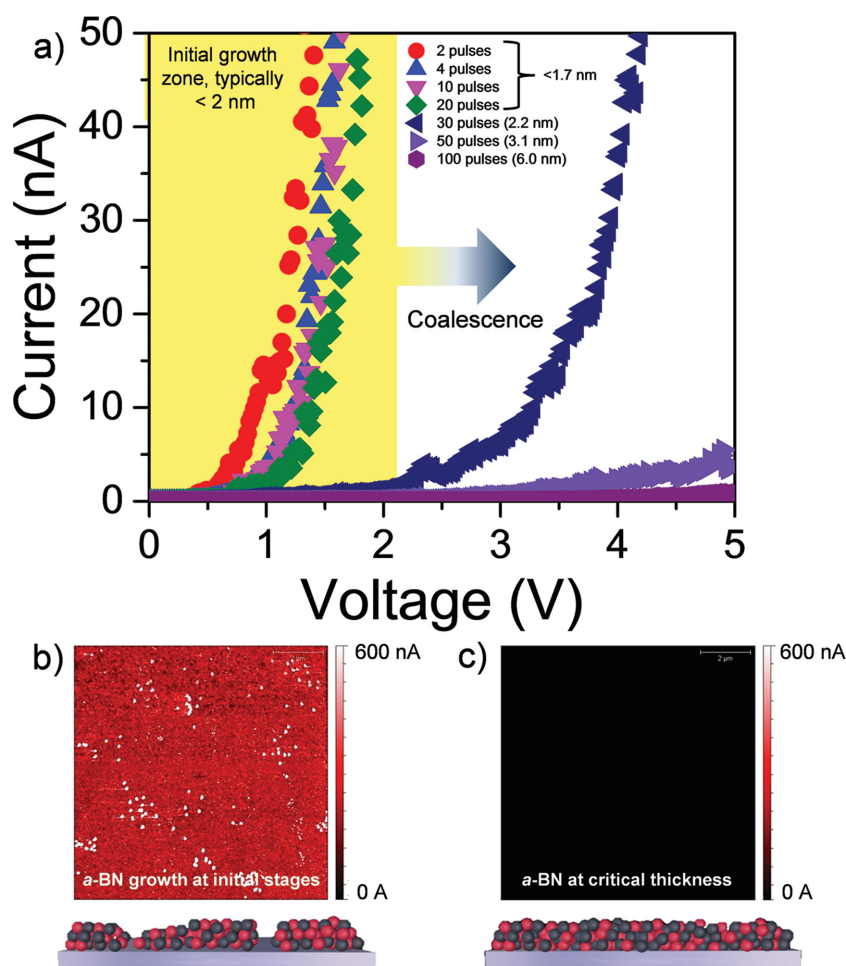

Figure 4. a) C-AFM *I–V* curves of *a*-BN on tungsten and corresponding number of laser pulses, b) C-AFM image and schematic of initial growth stages at 2 pulses, and c) C-AFM image and schematic of cohesive *a*-BN film at critical thickness of 20 pulses; scan sizes are 10 µm × 10 µm.

Materials
Views
www.MaterialsViews.com

ADVANCED
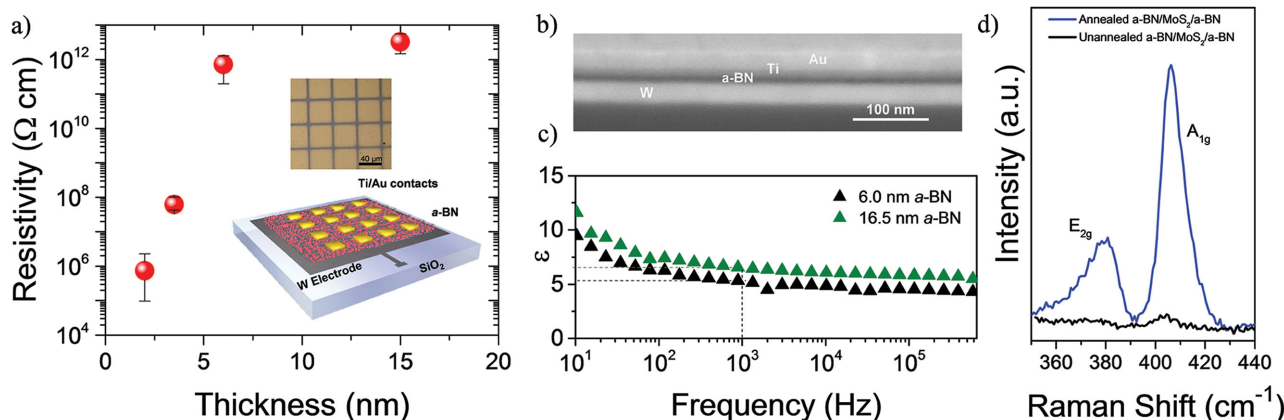FUNCTIONAL
MATERIALS
www.afm-journal.de

FULL PAPER

Figure 5. a) Electrical resistance measurements of continuous *a*-BN films on metallic tungsten at different thicknesses using 40 μm × 40 μm Ti/Au contacts seen in the inset, b) cross-sectional image of the 6 nm *a*-BN device, c) dielectric constant measurements for 6 nm and 16.5 nm films, and d) MoS$_2$ Raman signature of as-deposited (black) and laser annealed (blue) in BN/MoS$_2$/BN heterostructured stack.

average resistivity values of 7.22×10^{11} ohm·cm at 6 nm thickness (100 laser pulses) and 2.98×10^{12} ohm·cm at 16.5 nm (200 laser pulses) were measured, which is near an expected value for a bulk BN film.[45]

In addition to resistivity, the same device was used for dielectric constant measurements of the 6 and 16.5 nm samples (Figure 5c). A dielectric constant of 3 ± 1.0 has been reported in a polycrystalline CVD film of 15–19 nm thickness,[33] as leakage pathways at the grain boundaries can lead to charge dissipation within the material. In highly dense 6 and 16.5 nm *a*-BN films grown at 200 °C the measured dielectric constants were 5.2 and 6.5 at 1 kHz, respectively, with an average of 5.9, which approaches the dielectric constant of pure, single crystal *h*-BN. An increase in dielectric constant can be attributed to higher resistivity of the film, approaching a bulk value, where the electrical properties are not as influenced by surface defects and other contaminant species. Device-scale dielectric breakdown measurements indicate an E_{BD} value of 9.1 MV cm^{-1} for the 2.2 nm sample, as presented in the Weibull distribution in Figure S3 in the Supporting Information, which is consistent with the constant current C-AFM measurements of breakdown strength. Subsequent testing on the thicker W/*a*-BN/metal contact devices were inconclusive, as the metal contacts failed consistently near 8 V by delamination before breakdown of the *a*-BN material occurred.

Finally, optical bandgap measurements were performed on an 8 nm *a*-BN film grown on Al$_2$O$_3$ (0001), and resulted in a measured absorption bandgap of 4.5 eV, as seen in Figure S4 in the Supporting Information. A bandgap of 4.5 eV is well within the reported values for thin film amorphous boron nitride of 3.8–5.05 eV, as compared in Table 1. The bandgap measured here for ultrathin *a*-BN is slightly below that of the hexagonal phase of boron nitride, as both the bulk single crystal and polycrystalline *h*-BN produced by CVD exhibit a bandgap of 5.2–5.9 eV. Efforts to model and understand electronic properties of *h*-BN have been well explored;[46,47] however, a comparable model for *a*-BN has yet to be fully developed. A reduction in band gap has been observed in other crystalline-to-amorphous phase transitions, as the amorphous phase results in both a reduction in coordination of the bonding species, as well as random orientation of atomic

orbitals.[48] The values for dielectric constant, dielectric breakdown strength, and bandgap of the *a*-BN material in this work are listed in Table 1, as presented earlier, along with a comparison to other state-of-the-art ultrathin BN dielectrics and thermally grown SiO$_2$ thin films. These values reported are higher than those of previously measured *a*-BN thicker films and are believed to be due to the defect-free, large area, atomic-scale roughness and stoichiometry tuned precisely to applications in nanoelectronic systems.

As discussed, significant advantages of the laser deposited *a*-BN films over traditional ultrathin or 2D dielectrics includes large area nucleation and coalescence on diverse substrates at low temperatures (<200 °C). To demonstrate these advantages, in addition to retention of optical transparency of heterodevices on a polymer substrate, an *a*-BN/amorphous MoS$_2$/*a*-BN heterostructure was synthesized on PDMS with low temperature PVD methods. The MoS$_2$ was grown via PVD[43] at a thickness of 10 nm, however, at much lower temperatures than described in the previous work, the resulting MoS$_2$ film was amorphous and insulating. Recent studies have proven successful in the laser annealing and crystallization of such amorphous MoS$_2$ layers by photonic curing on a flexible PDMS substrate.[49] In the study presented here, a 514 nm laser was used to crystallize the amorphous MoS$_2$ into the 2H phase through the transparent *a*-BN film of approximately 2 nm, evidenced by the E2g and A1g characteristic peaks of MoS$_2$ in Figure 5 d and no observable damage to the dielectric *a*B-N film. This capability is an important advantage in low-temperature processing of 2D materials, as the crystallization of MoS$_2$ sandwiched between low-temperature grown *a*-BN layers will significantly hinder oxidation of the environmentally sensitive MoS$_2$, and allow for direct-write manufacturing of MoS$_2$ transistors on flexible substrates with well-defined gate dielectrics and without degradation from exposure to the ambient environment.

3. Conclusion

The new low-temperature processing route towards ultrathin and continuous *a*-BN described in this work represents a

FULL PAPER

significant breakthrough in dielectric processing necessary for next-generation 2D material heterostructure systems. The *a*-BN ultrathin dielectric material deposited at 200 °C is universal in structure and chemistry on numerous substrates including flexible PDMS, traditional insulating electronic substrates such as SiO_2 and Al_2O_3, other 2D materials including graphene, 2D MoS_2, and conducting metals. A dielectric constant of 5.9 ± 0.7 at 1 kHz and breakdown voltage of 9.8 ± 1.0 MV cm^{-1} were measured for *a*-BN films, representing values higher than previously reported for CVD *h*-BN and close to that of single crystal *h*-BN, as shown in Table 1. The electronic properties of ultrathin continuous *a*-BN produced by PLD, coupled with the versatility in materials processing and adaptability, the optical transparency, as well as the large-area and uniform coverage at low temperatures, make integration of *a*-BN into 2D nanoelectronic systems and devices a very exciting and appealing possibility.

4. Experimental Section

Growth: Growth of amorphous boron nitride films were performed in an ultrahigh vacuum chamber from a 248 nm KrF laser at 1 Hz repetition rate, a laser power of 900 mJ pulse^{-1}, and spot size of 2.66 mm × 1.5 mm, corresponding to a laser energy of 22.5 J cm^{-2}. Depositions were performed at a working distance of 3 cm with an amorphous boron nitride target and the chamber was filled with 99.9999% N_2 gas at a pressure of 50 mTorr.

Tungsten films for bottom electrodes were grown in the same chamber with DC magnetron sputtering at a power of 40 W applied to the target, 2.5 mTorr of argon background pressure and an argon flow rate at 30 sccm on an SiO_2/Si wafer. Titanium/gold contacts were grown in a similar manner, with 40 W applied to the titanium and gold targets sequentially, and an argon pressure of 15 mTorr.

Chemical and Structural Analysis: X-ray photoelectron spectroscopy (XPS) was carried out using a Kratos AXIS Ultra spectrometer with a monochromatic Al Kα X-ray source (1486.6 eV) operated at 120 W (12 kV, 10 mA) and at approximately 4×10^{-9} Torr. Survey scans were collected over the binding energy range of −5 to 1200 eV, in 1 eV steps, using a dwell time of 400 ms and analyzer pass energy of 160 eV. High resolution spectra of the B *1s* and N *1s* regions were acquired using an energy step size of 0.1 eV, a dwell time of 500 ms, and analyzer pass energy of 20 eV. XPS spectra were analyzed using the CasaXPS software. Peak areas were determined using a Shirley background subtraction. The binding energy was calibrated to Al 2p at 74.5 eV where sapphire was present and to Si 2p at 102.4 eV where PDMS was present.

The cross-sectional TEM of BN thin films was performed using a FEI Nova focused ion beam (FIB) microscope equipped with an Omniprobe manipulator for lift out. Samples were studied in a FEI Titan 80–300 S/TEM operating at 300 kV, which was equipped with a Cs corrector for high-resolution imaging. In addition, cross-sectional microscopy was used in measuring film thickness, and the scatter in the measurements is reflected in Table 1.

Device Characterization: Resistivities were measured using a Keithley 4200 analyzer with a thin gold filament to make contact onto a 40 μm × 40 μm gold top electrode to facilitate the measurement. Dielectric permittivity characterizations were performed using a Novocontrol Alpha Analyzer. Scans were conducted at discrete frequencies, swept over the range of 10 Hz–1 MHz, at an AC driving voltage of 100 mV.

Supporting Information

Supporting Information is available from the Wiley Online Library or from the author.

[1] A. K. Geim, I. V. Grigorieva, *Nature* **2013**, *499*, 419.

[2] G. Fiori, F. Bonaccorso, G. Iannaccone, T. Palacios, D. Neumaier, A. Seabaugh, S. K. Banerjee, L. Colombo, *Nat. Nano* **2014**, *9*, 768.

[3] A. Hsu, W. Han, C. S. Yong, B. Mailly, Z. Xu, Y. Lili, S. Yumeng, H. L. Yi, M. Dubey, K. K. Ki, K. Jing, T. Palacios, *Proc. IEEE* **2013**, *101*, 1638.

[4] T. Roy, M. Tosun, J. S. Kang, A. B. Sachid, S. B. Desai, M. Hettick, C. C. Hu, A. Javey, *ACS Nano* **2014**, *8*, 6259.

[5] D. Jariwala, V. K. Sangwan, L. J. Lauhon, T. J. Marks, M. C. Hersam, *ACS Nano* **2014**, *8*, 1102.

[6] D. Akinwande, presented at *Micro Nanotechnol. Sens., Syst. Appl. VI*, May 2014.

[7] M. Osada, T. Sasaki, *Adv. Mater.* **2012**, *24*, 210.

[8] S. Wolf, R. N. Tauber, in *Silicon Processing for the VLSI Era: Volume 1—Process Technology*, Lattice Press, Sunset Beach, CA, USA **2000**, 265.

[9] S. Kamiyama, T. Miura, Y. Nara, *Appl. Phys. Lett.* **2005**, *87*, 1.

[10] D. Gu, K. Tapily, P. Shrestha, M. Y. Zhu, G. Celler, H. Baumgart, *J. Electrochem. Soc.* **2008**, *155*, G129.

[11] S. M. George, *Chem. Rev.* **2010**, *110*, 111.

[12] L. Lei, Y. P. Feng, Z. X. Shen, *Phys. Rev. B Condens. Matter Mater. Phys.* **2003**, *68*, 104102.

[13] R. Zedlitz, M. Heintze, M. B. Schubert, *J. Non-Crystall. Solids* **1996**, *198–200*, 403.

[14] M. J. Rand, J. F. Roberts, *J. Electrochem. Soc.* **1968**, *115*, 423.

[15] K. Watanabe, T. Taniguchi, H. Kanda, *Nat. Mater.* **2004**, *3*, 404.

[16] A. Soltani, A. Talbi, V. Mortet, A. BenMoussa, W. J. Zhang, J. C. Gerbedoen, J. C. De Jaeger, A. Gokarna, K. Haenen, P. Wagner, presented at *2010 Wide Bandgap Cubic Semiconductors: from Growth to Devices: E-MRS Symposium F, 8 June–10 Oct.* **2010**.

[17] Z. Liu, Y. Gong, W. Zhou, L. Ma, J. Yu, J. C. Idrobo, J. Jung, A. H. MacDonald, R. Vajtai, J. Lou, P. M. Ajayan, *Nat. Commun.* **2013**, *4*, 2541.

[18] V. L. Solozhenko, V. Z. Turkevich, W. B. Holzapfel, *J. Phys. Chem. B* **1999**, *103*, 2903.

[19] Y. Shi, C. Hamsen, X. Jia, K. K. Kim, A. Reina, M. Hofmann, A. L. Hsu, K. Zhang, H. Li, Z. Y. Juang, M. Dresselhaus, L. J. Li, J. Kong, *Nano Lett.* **2010**, *10*, 4134.

[20] K. K. Kim, A. Hsu, X. Jia, S. M. Kim, Y. Shi, M. Hofmann, D. Nezich, J. F. Rodriguez-Nieva, M. Dresselhaus, T. Palacios, J. Kong, *Nano Lett.* **2012**, *12*, 161.

[21] N. Guo, J. Wei, L. Fan, Y. Jia, D. Liang, H. Zhu, K. Wang, D. Wu, *Nanotechnology* **2012**, 23.

[22] R. Y. Tay, M. H. Griep, G. Mallick, S. H. Tsang, R. S. Singh, T. Tumlin, E. H. T. Teo, S. P. Karna, *Nano Lett.* **2014**, *14*, 839.

[23] G. E. Wood, A. J. Marsden, J. J. Mudd, M. Walker, M. Asensio, J. Avila, C. Kai, G. R. Bell, N. R. Wilson, *2D Mater.* **2015**, *2*, 025003.

Materials
Views

www.MaterialsViews.com

ADVANCED
FUNCTIONAL
MATERIALS

www.afm-journal.de

[24] A. B. Preobrajenski, A. S. Vinogradov, N. Martensson, *Surf. Sci.* **2005**, *582*, 21.

[25] N. A. Vinogradov, A. A. Zakharov, M. L. Ng, A. Mikkelsen, E. Lundgren, N. Martensson, A. B. Preobrajenski, *Langmuir* **2012**, *28*, 1775.

[26] Y. Zhang, X. Weng, H. Li, H. Li, M. Wei, J. Xiao, Z. Liu, M. Chen, Q. Fu, X. Bao, *Nano Lett.* **2015**, *15*, 3616.

[27] A. Goriachko He, M. Knapp, H. Over, M. Corso, T. Brugger, S. Berner, J. Osterwalder, T. Greber, *Langmuir* **2007**, *23*, 2928.

[28] M. Morscher, M. Corso, T. Greber, J. Osterwalder, *Surface Science* **2006**, *600*, 3280.

[29] J. H. Park, J. C. Park, S. J. Yun, H. Kim, D. H. Luong, S. M. Kim, S. H. Choi, W. Yang, J. Kong, K. K. Kim, Y. H. Lee, *ACS Nano* **2014**, *8*, 8520.

[30] M. S. Bresnehan, M. J. Hollander, M. Wetherington, K. Wang, T. Miyagi, G. Pastir, D. W. Snyder, J. J. Gengler, A. A. Voevodin, W. C. Mitchel, J. A. Robinson, *J. Mater. Res.* **2014**, *29*, 3.

[31] T. A. Friedmann, K. F. McCarty, E. J. Klaus, J. C. Barbour, W. M. Clift, H. A. Johnsen, D. L. Medlin, M. J. Mills, D. K. Ottesen, *Thin Solid Films* **1994**, *237*, 48.

[32] S. L. Rumyantsev, M. E. Levinshtein, A. D. Jackson, S. N. Mohammad, G. L. Harris, M. G. Spencer, M. S. Shur, *Properties of Advanced Semiconductor materials: GaN, AlN, InN, BN, SiC, SiGe*, (Eds: M. E. Levinshtein, S. L. Rumyantsev, M. S. Shur), John Wiley & Sons, New York, NY, USA **2001**, 67.

[33] K. K. Kim, A. Hsu, X. Jia, S. M. Kim, Y. Shi, M. Dresselhaus, T. Palacios, J. Kong, *ACS Nano* **2012**, *6*, 8583.

[34] C. M. Orofeo, S. Suzuki, H. Hibino, *J. Phys. Chem. C* **2014**, *118*, 3340.

[35] G. H. Lee, Y. J. Yu, C. Lee, C. Dean, K. L. Shepard, P. Kim, J. Hone, *Appl. Phys. Lett.* **2011**, *99*, 243114.

[36] Y. Hattori, T. Taniguchi, K. Watanabe, K. Nagashio, *ACS Nano* **2014**, *9*, 916.

[37] S. N. Mohammad, F. J. Kub, J. Eddy, *J. Vac. Sci. Technol. B:Nanotechnol. Microelectron.* **2011**, *29*, 021021.

[38] N. R. Glavin, M. L. Jespersen, M. H. Check, J. Hu, A. M. Hilton, T. S. Fisher, A. A. Voevodin, *Thin Solid Films* **2014**, *572*, 245.

[39] N. R. Glavin, C. Muratore, M. L. Jespersen, J. Hu, T. S. Fisher, A. A. Voevodin, *J. Appl. Phys.* **2015**, 117.

[40] J. Greer, in *Pulsed Laser Deposition of Thin Films: Applications-Led Growth of Functional Materials* (Ed: Robert Eason), Wiley-Interscience, Hoboken, NJ, USA **2006**, 191.

[41] M. Panzner, R. Dietsch, T. Holt, H. Mai, S. Vollmar, presented at *Laser Ablat. Symp. F: Third Int. Symp. Laser Ablat. (COLA'95) 1995 E-MRS Spring Conf., 22–26 May 1995*, Netherlands, **1996**.

[42] NIST X-Ray Photoelectron Spectroscopy Database, http://srdata.nist.gov/xps, accessed: 2012.

[43] C. Muratore, J. J. Hu, B. Wang, M. A. Haque, J. E. Bultman, M. L. Jespersen, P. J. Shamberger, M. E. McConney, R. D. Naguy, A. A. Voevodin, *Appl. Phys. Lett.* **2014**, *104*, 261604.

[44] K. Boucart, A. M. Ionescu, *Solid-State Electron. Res. Conf.* **2008**, *52*, 1318.

[45] C. Steinborn, M. Herrmann, U. Keitel, A. Schonecker, J. Rathel, D. Rafaja, J. Eichler, *J. Eur. Ceram. Soc.* **2013**, *33*, 1225.

[46] J. Wu, B. Wang, Y. Wei, R. Yang, M. Dresselhaus, *Mater. Res. Lett.* **2013**, *1*, 200.

[47] P. Miro, M. Audiffred, T. Heine, *Chem. Soc. Rev.* **2014**, *43*, 6537.

[48] A. De Jamblinne de Meux, G. Pourtois, J. Genoe, P. Heremans, *J. Phys. D: Appl. Phys.* **2015**, *48*, 435104.

[49] M. E. McConney, T. Shelton, R. E. Stevenson, J. E. Bultman, J. Hu, M. L. Jespersen, N. R. Glavin, A. T. Juhl, M. F. Durstock, J. G. Colborn, M. H. Check, M. K. Gupta, A. Haque, R. D. Naguy, A. A. Voevodin, C. Muratore, unpublished.